International Research Journal of Advanced Engineering and Science
ISSN (Online): 2455-9024

Effects of Process Parameters on Single-Track Formation in Directed Laser Metal Deposition of AlSi10Mg Alloy

Nguyen Ba Bao[1], Nguyen Van Quan[1], Vu Van Quang[2], Doan Van Phuc[3], Nguyen Duc Long[4]
Trinh Quang Hung[1*]
[1]Faculty of Mechanical Engineering, Le Quy Don Technical University, Ha Noi, Viet Nam
[2]School of Mechanical Engineering, Ha Noi University of Science and Technology, Ha Noi, Viet Nam
[3]Institute of Chemistry and Material, Academy of Military Science and Technology, Ha Noi, Viet Nam
[4]Faculty of Practical Training, Tran Dai Nghia University, Ho Chi Minh, Viet Nam
[*]Corresponding author: trinhquanghung@lqdtu.edu.vn

***Abstract*— *This study investigates the influence of laser power and scanning speed on the single-track geometry of AlSi10Mg processed via Directed Laser Metal Deposition (DLMD). A 2×2 full factorial experimental design was employed to systematically evaluate the effects and interactions of these parameters. Statistical analysis through ANOVA revealed that laser power is the most dominant and statistically significant factor influencing track geometry. Scanning Electron Microscopy (SEM) images confirmed stable, semi-elliptical track profiles with good metallurgical bonding at the track/substrate interface, though gas-induced porosity was observed. Microhardness measurements showed a clear distinction between regions, with the cladding region exhibiting an average hardness of 111 HV, significantly higher than the substrate and comparable to previously reported values for similar conditions, while the bonding region maintained a value of approximately 74 HV. These findings highlight the critical role of laser power in determining melt pool behavior and track morphology, supporting process optimization for high-quality DLMD fabrication of AlSi10Mg components.*

***Keywords*— *Laser powr; scanning speed; directed laser metal deposition; single track; AlSi$_{10}$Mg alloy.*

I. Introduction

AlSi10Mg, a hypoeutectic aluminum alloy from the Al-Mg-Si series, is widely utilized in the aerospace and automotive industries due to its light weight, favorable mechanical properties, and cost-effective recyclability [1]. Components made from AlSi$_{10}$Mg, particularly those with large dimensions and complex geometries, are typically manufactured through conventional casting processes. However, casting is associated with limitations, including prolonged production times and significant material wastage [2]. Directed Laser Metal Deposition (DLMD), an advanced additive manufacturing (AM) technique, offers a promising alternative for fabricating metal components [3]. Also known by various terms such as Direct Metal Deposition (DMD), Directed Energy Deposition (DED), Laser Metal Deposition (LMD), and Direct Laser Deposition (DLD), DLMD enables the rapid and cost-efficient production, repair, and restoration of parts, molds, and tools directly from 3D CAD models. This technology accommodates a broad range of metals, including those challenging to machine conventionally or requiring intricate geometries, and is particularly effective for depositing exceptionally hard coatings. Components produced via DLMD exhibit superior mechanical properties, characterized by minimal porosity and robust adhesion to the substrate [4].

Previous research has explored the capabilities of DLMD for AlSi10Mg fabrication. Chen et al. [1] investigated the microstructure and microhardness of AlSi10Mg components manufactured using DMD, reporting mechanical properties surpassing those of cast counterparts, thus affirming the suitability of DMD for this alloy. Javidani et al. [5] examined the microstructure and microhardness of AlSi10Mg processed via DED, though their study did not extend to mechanical property evaluation. Wang et al. [6] analyzed the microstructure and microhardness of AlSi10Mg fabricated by LMD, demonstrating successful deposition of thin-walled specimens without cracks or concave deformation; however, they noted reduced homogeneity with increasing energy input. Fei et al. [7] explored the mechanical properties of AlSi10Mg produced by LMD and assessed the effects of post-deposition heat treatment. To date, studies have predominantly focused on variations in microstructure and mechanical properties along the height of deposited structures, such as thin walls and bulk forms, or individually assessed the influence of parameters like laser power and scanning speed.

This study investigates the effects of laser power and scanning speed on the geometry of single-track AlSi10Mg deposits produced by DLMD. The process parameters were simultaneously varied to evaluate their influence on track width and penetration depth. Analysis of Variance (ANOVA) was employed to assess the statistical significance of individual effects and possible interactions, followed by regression modeling to establish predictive relationships between inputs and outputs. Additionally, microhardness and microstructural analyses were conducted to provide further insight into the material characteristics of the DLMD-fabricated AlSi10Mg alloy.

II. Materials and Methods

The experiments were carried out utilizing the facilities shown in Fig. 1. The experimental setup consisted of a fiber laser with a maximum output power of 500 W (YLR-500-WC-Y14, IPG Photonics), a pressure-type powder feeder, a continuous coaxial powder nozzle, a three-axis worktable, and an integrated control system. Prior to each deposition, the chamber was evacuated using a vacuum pump and subsequently purged thoroughly with nitrogen (N_2) gas until the oxygen concentration was reduced to below 100 ppm. N_2 gas was also used as both shielding and carrier gases to protect the metal molten pool from oxidation and to deliver the AlSi10Mg alloy powder into the molten pool. The flow rates for the carrier and shielding gases were maintained at 3.5 L/min and 5.5 L/min, respectively. The laser beam was focused to a diameter of 1.0 mm using a focusing lens with a focal length of 190 mm and was positioned at a standoff distance of 9 mm from the nozzle to the substrate.

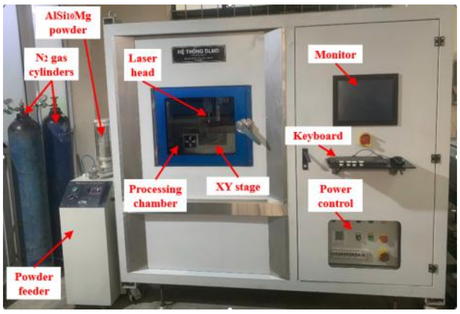

Fig. 1. The DLMD system.

TABLE 1. Chemical composition of 6061 Aluminum alloy substrate

% Si	% Fe	% Cu	% Mn	% Al
0.4-0.8	≤ 0.7	0.15-0.4	≤ 0.15	
% Mg	%Cr	% Zn	% Ti	Bal.
0.8-1.2	0.04-0.35	≤ 0.25	≤ 0.15	

TABLE 2. Chemical composition of AlSi10Mg alloy powder

% Al	% Si	% Fe	% Cu	% Mn	% Mg
89.47	9.13	0.26	0.008	0.31	0.28
% Zn	% Ni	% Ti	% Sn	% Pb	% Other
0.008	0.015	0.1	0.003	0.001	0.41

The substrate was a 6061 aluminum alloy plate, measuring 150×150×5 mm, with its chemical composition detailed in TABLE 1. The powder employed, AlSi10Mg alloy, was characterized by a particle size range of 45-100 µm, and its composition is specified in

TABLE 2. Prior to experimentation, the AlSi10Mg powder was dried in an oven at 200°C for 30 minutes to eliminate residual moisture content. The substrate was mechanically polished with sandpaper and subsequently cleaned with acetone to remove surface contaminants, thereby enhancing adhesion to the deposited layer.

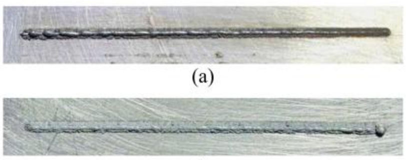

(b)

Fig. 2. Single tracks deposited under the following process conditions: (a) laser power of 300 W and scanning speed of 360 mm/min, and (b) laser power of 400 W and scanning speed of 360 mm/min (powder feed rate: 2.4 g/min).

Process parameters, including laser power (*P*) and scanning speed (*V*), each at two levels, were configured according to a two-level factorial design. The powder feed rate was fixed at 2.4 g/min. Each combination of input parameters was replicated once, resulting in a total of eight experimental runs. The corresponding values and measured outcomes, namely the width (*W*) and penetration depth (*D*) of the single tracks, are presented in TABLE 3. Representative optical images of the deposited tracks are shown in Fig. 2.

Following deposition, the samples were separated from the substrate using wire electrical discharge machining (EDM) to produce cross-sectional specimens of the single tracks. The cross-sections were ground with SiC abrasive paper, progressing through grit sizes ranging from 240 to 2000. Subsequently, the samples were mechanically polished using a polishing machine (METASERV 2000, Spectrographic, UK). The polished specimens were then etched for 15 seconds with a solution consisting of 1.0 ml HF, 1.5 ml HCl, 2.5 ml HNO_3, and 90 ml distilled water.

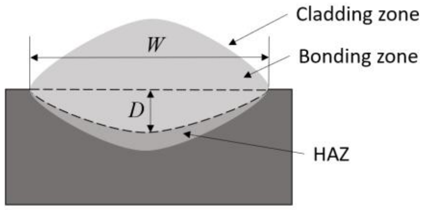

Fig. 3. The geometric parameters of the single tracks

The metallographic samples were analyzed with an optical microscope (Axio Observer.D1m, Zeiss). Their geometric parameters (Fig. 3) were quantified using AxioVision Rel. 4.8 software. Microstructural analyses were conducted with a scanning electron microscope (SEM) (TM4000Plus, Hitachi). Vickers hardness measurements were performed on a Vickers micro-hardness tester (DM2D, Affri, Italy) under a 100 g load with a 10-second indentation dwell time.

TABLE 3. The input parameters and experimental outcomes

Std	Run	*P* (W)	*V* (mm/min)	*F* (g/min)	*W* (µm)	*D* (µm)
7	1	400	360	2.4	929.44	154.46
1	2	300	240	2.4	793.69	62.33
8	3	400	360	2.4	926.48	154.41
4	4	400	240	2.4	942.98	156.29
5	5	300	360	2.4	753.84	58.72
6	6	300	360	2.4	701.18	53.59
2	7	300	240	2.4	784.57	69.03
3	8	400	240	2.4	984.15	161.24

III. RESULT AND DISCUSSION

A. *Track morphology*

The geometry of the resulting single-track depositions is illustrated in Fig. 2. A regular normal track height was observed in samples processed at high level of laser power. In contrast, samples produced at a low laser power often exhibited insufficient overlap between clad beads, resulting in an irregular ball-shaped morphology.

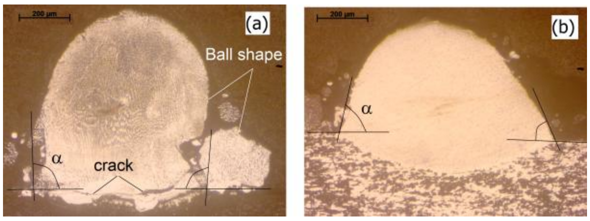

Fig. 4. Optical images showing (a) ball-shaped and (b) normal morphology at the low and high laser level, respectively (scanning speed: 360 mm/min).

It can be seen from Fig. 4 that the wetting angle of the clad bead, α, is significantly larger for the ball-shaped track compared to the normal one. This can be attributed to the fact that, at 300 W, the substrate material in the bonding zone was not fully melted, resulting in weak metallurgical interaction and, consequently, a large wetting (or contact) angle of the clad bead.

B. *Effect of process parameters on the track width*

The ANOVA results for single-track width are presented in **Error! Reference source not found.**. The model F-value of 44.09 indicates that the model is statistically significant. There is only a 0.16% probability that such a high F-value could occur due to random noise.

TABLE 4. ANOVA analysis of the track width model.

Source	Sum of Squares	df	Mean Square	F-value	p-value	
Model	75355,00	3	25118,33	44,09	0,0016	significant
P	70312,50	1	70312,50	123,41	0,0004	
V	4704,50	1	4704,50	8,26	0,0453	
$P\times V$	338,00	1	338,00	0,5932	0,4841	
Pure Error	2279,00	4	569,75			
Cor Total	77634,00	7				

The analysis identifies laser power (P) as the dominant and statistically significant factor, with an F-value of 123.41 and a p-value well below 0.05. Scanning speed (V) is also statistically significant but has only a minor effect on track width. However, their interaction ($P\times V$) is not statistically significant and exhibits a negligible F-value. This suggests that, within the tested range, the influence of scanning speed is overshadowed by that of laser power, likely due to the direct control of laser over the energy delivered to the substrate and powder, affecting melt pool size and deposition behavior. This is consistent with prior studies linking laser power to geometric outcomes in laser-based additive processes [8, 9, 10].

TABLE 5. Fit Statistics from ANOVA analysis of the track width model.

Std. Dev.	23,87	R^2	0,9706
Mean	851,50	**Adjusted R^2**	0,9486
C.V. %	2,80	**Predicted R^2**	0,8826
		Adeq Precision	13,9825

The model achieves a coefficient of determination (R^2) of 0,9706 (see TABLE 5), explaining 97,06% of the variability in single-track width, while an adjusted R^2 of 0.9486 further confirms a robust fit. An adequate precision ratio of 13,9825 (well above 4) reflects a strong signal-to-noise ratio, reinforcing the model's reliability.

Following the ANOVA analysis, linear regression equations were derived to model the relationship between the factors and single-track width. The coded linear regression equation:

$$W = 851.50 + 93.75\times P - 24.25\times V \quad (1)$$

where P and V are the coded levels (–1 or +1) of laser power and scanning speed, respectively. The coefficients reveal that laser power exerts a substantial positive effect (93.75) on track width, with higher power leading to a wider track, while scanning speed has a smaller negative effect (–24.25). Increasing scanning speed reduces interaction time, thereby decreasing melting efficiency. Given the extremely high laser reflectivity and thermal conductivity of aluminum-based materials, it is evident that a high laser power density is necessary to generate a stable molten pool. This explains the dominant influence of laser power on molten pool development and track formation.

The linear regression equation, expressed in terms of actual experimental units, is presented in Eq. (2).

$$W = 316.50 + 1.875\times P - 0.404\times V \quad (2)$$

Here, P ranges from 300 to 400 W and V from 240 to 360 mm/min, reflecting the tested levels. This equation allows direct prediction of track width based on specific laser power and scanning speed settings within the experimental range.

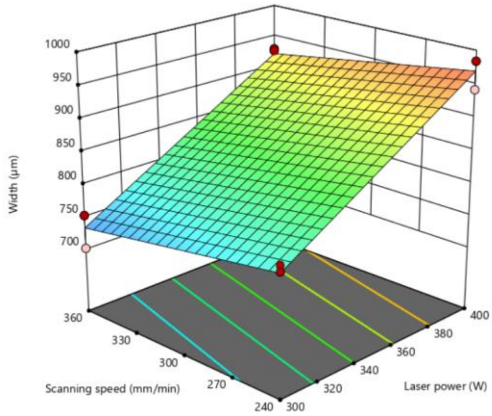

Fig. 5. Effect of laser power and scanning speed on track width.

The 3D surface plot illustrating the combined influence of laser power and scanning speed on single-track width is shown in **Error! Reference source not found.**. The plot, covering a laser power range of 300 to 400 W and a scanning speed of 240 to 360 mm/min, highlights the dominant positive effect of laser power and the comparatively minor negative effect of scanning speed, which is in alignment with the regression coefficients.

C. *Effect of processing parameters on track penetration depth*

The ANOVA analysis for track penetration depth (D) closely mirrors that of track width, with laser power identified as the dominant factor and scanning speed exhibiting a minor effect, while their interaction remains statistically insignificant. Building on this similarity, linear regression equations were derived to model the relationship between P, V, and track depth in the 2×2 factorial design. The coded equation, using normalized levels (–1 and +1), and the actual equation, in experimental units, are presented below to quantify the effects and enable prediction of track depth across the tested range.

Nguyen Ba Bao, Nguyen Van Quan, Vu Van Quang, Doan Van Phuc, Nguyen Duc Long, and Trinh Quang Hung "Effects of Process Parameters on Single-Track Formation in Directed Laser Metal Deposition of AlSi10Mg Alloy" *International Research Journal of Advanced Engineering and Science,* Volume 10, Issue 2, pp. 70-74, 2025.

The coded linear regression equation for track depth:

$$D = 108.38 + 47.88 \times P - 3.63 \times V \quad (3)$$

This indicates a strong positive effect of laser power (47.88) and a slight negative effect of scanning speed (–3.63, consistent with the ANOVA results.

The actual linear regression equation:

$$D = -160.50 + 0.82 \times P - 0.22 \times V \quad (4)$$

Here, P ranges from 300 to 400 W and V from 240 to 360 mm/min, reflecting the experimental conditions. To further illustrate these relationships, a 3D surface plot (Fig. 6) visualizes the variation in track depth, D, as a function of P and V, highlighting the pronounced influence of laser power and the subtle decline with increasing scanning speed, without considering their interaction.

TABLE 6. ANOVA result relative depth model

Source	Sum of Squares	df	Mean Square	*F*-value	*p*-value	
Model	18456,38	3	6152,13	497,14	< 0.0001	significant
P	18336,13	1	18336,13	1481,71	< 0.0001	
V	105,13	1	105,13	8,49	0,0435	
P×*V*	15,13	1	15,13	1,22	0,3309	
Pure Error	49,50	4	12,37			
Cor Total	18505,88	7				

The regression equations reveal that laser has a strong positive effect on both track width and depth, with coefficients of 1.875 and 0.82, respectively, indicating a greater influence on track width (2.29 times stronger per watt). Scanning speed exerts a negative effect on both, with coefficients of -0.404 for W and -0.22 for D, showing a larger reduction in W (1.84 times stronger per mm/s). Within each response, P dominates over V, with its effect on W being 4.6 (≈ 1.875 / 0.404) times greater than V's, and on D 3.7 (≈ 0.82 / 0.22) times greater. These trends suggest that track width is more sensitive to changes in both factors, while track depth exhibits a more moderate response, likely due to the high reflectivity and thermal conductivity of the material, limiting energy penetration.

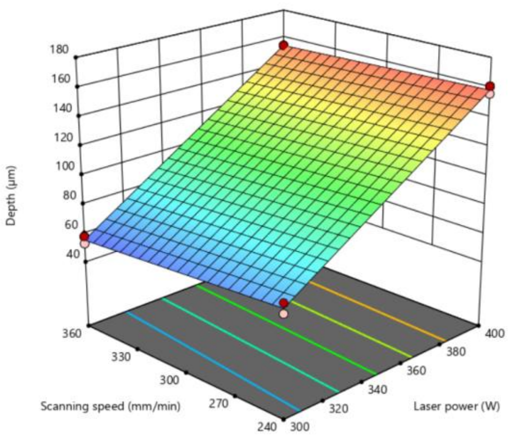

Fig. 6. Effect of processing parameters on the track penetration depth.

D. Microstructural analysis and defects of single tracks

Fig. 7 presents SEM images detailing the microstructural features and defects of a single track on AlSi10Mg, processed at a laser power of 400 W and a scanning speed of 360 mm/min. Fig. 7a reveals a stable, semi-elliptical track, indicative of conduction-mode melting and effective fusion with the substrate, ensuring good bonding.

Fig. 7b and 7c shows rough internal surfaces, suggestive of gas pores in the top and central regions. These defects are likely caused by the vaporization of elements such as magnesium or the entrapment of shielding gas. At high laser power (400 W), possible keyhole instability combined with rapid solidification, driven by the high thermal conductivity of AlSi10Mg, can exacerbate pore formation and trap them within the solidified material. Such pores act as stress concentrators, reducing tensile strength, ductility, and fatigue life. Additionally, at lower laser power settings (300 W), as observed in Fig. 4a, microcracks emerge due to insufficient energy for proper melting, further complicating defect management.

Fig. 7d confirms a pore-free track bottom region and a crack-free track/substrate interface, demonstrating strong bonding. This is supported by the track's fine microstructure, a result of rapid cooling, which enhances mechanical properties while ensuring effective fusion with the substrate. Previous studies have also reported the occurrence of crack-free yet porous AlSi10Mg deposits processed via DLMD and laser bed fusion method [6, 11].These findings highlight the potential of DLMD processing for AlSi10Mg but underscore the need to optimize laser power and scanning speed as well as other process parameters to minimize defects.

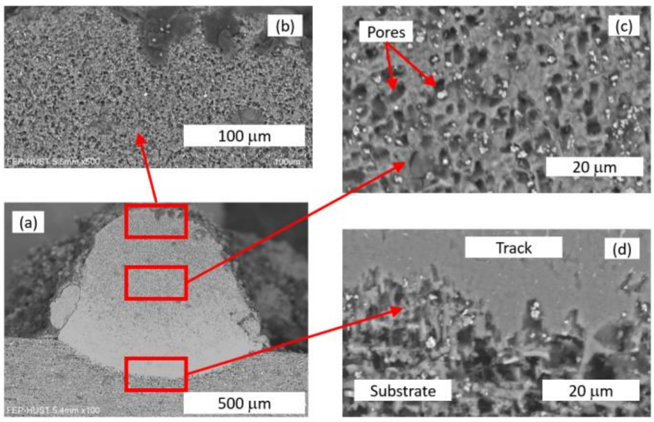

Fig. 7. Microstructure of the specimen

E. Single track microshardness properties

Microhardness tests were performed to evaluate the hardness distribution along the track fabricated at a laser power of 400 W and a scanning speed of 240 mm/min. Measurements were taken at six positions along the track height, as illustrated in Fig. 8. The results given in Fig. 9 reveal two distinct regions: a hard cladding region (positions 1, 2, and 3) and a softer bonding region (positions 4, 5, and 6). The microhardness remains relatively consistent within each region. The clad region exhibits an average hardness of approximately 111 HV, which is higher than the values reported by Gao and Tan for AlSi10Mg powder processed using DLMD [12, 13]. In contrast, the bonding region shows an average hardness of about 74 HV, which is comparable to that of the substrate.

International Research Journal of Advanced Engineering and Science
ISSN (Online): 2455-9024

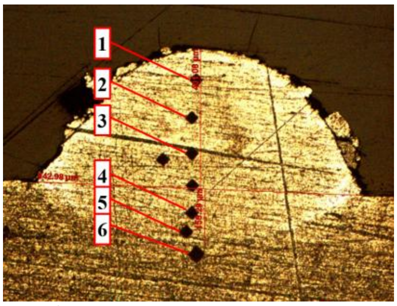

Fig. 8. Positions of microhardness measurement along the track height (process conditions: 400 W and 240 mm/min).

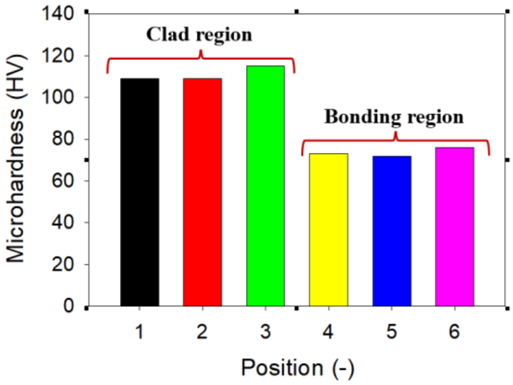

Fig. 9. Microhardness of a single track processed under conditions of 400 W and 240 mm/min.

IV. Conclusion

This study investigated the effects of laser power and scanning speed on the AlSi10Mg single track geometry using a 2×2 factorial design, complemented by SEM and microhardness analyses to evaluate microstructural features, mechanical properties, and defects. The ANOVA analysis revealed that laser power is the dominant factor influencing both track width and penetration depth, with a stronger effect on width, while scanning speed has a minor, negative impact, reducing both dimensions due to decreased interaction time.

SEM analysis confirmed a stable, semi-elliptical track geometry characteristic of conduction-mode melting, with good metallurgical bonding at the track/substrate interface. The presence of a fine microstructure, attributed to rapid solidification, further supports the quality of the deposition. However, gas porosity was observed throughout the track. Microhardness measurements revealed a distinct variation across regions: the clad exhibited a higher average hardness of 111 HV, while the bonding region averaged 74 HV, comparable to the substrate. These results demonstrate effective processing and a well-formed interface in the DLMD-fabricated track.

The findings highlight the potential of laser processing for AlSi10Mg in additive manufacturing, but underscore the need for precise parameter optimization to minimize defects while preserving desirable microstructural properties.

References

[1] B. Chen, Y. Yao, X. Song, C. Tan, L. Cao, and J. Feng, "Microstructure and mechanical properties of additive manufacturing AlSi10Mg alloy using direct metal deposition," *Ferroelectrics*, vol. 523, no. 1, pp. 153–166, 2018, doi: 10.1080/00150193.2018.1392147.

[2] P. Kiani, A. D. Dupuy, K. Ma, and J. M. Schoenung, "Directed energy deposition of AlSi10Mg: Single track nonscalability and bulk properties," *Mater. Des.*, vol. 194, p. 108847, 2020, doi: 10.1016/j.matdes.2020.108847.

[3] P. Ghosal, M. C. Majumder, and A. Chattopadhyay, "Study on direct laser metal deposition," *Mater. Today Proc.*, vol. 5, no. 5, pp. 12509–12518, 2018, doi: 10.1016/j.matpr.2018.02.232.

[4] A. Angelastro, S. L. Campanelli, G. Casalino, A. D. Ludovico, and S. Ferrara, "A methodology for optimization of the Direct Laser Metal Deposition process," *Key Eng. Mater.*, vol. 473, pp. 75–82, 2011, doi: 10.4028/www.scientific.net/KEM.473.75.

[5] M. Javidani, J. Arreguin-Zavala, J. Danovitch, Y. Tian, and M. Brochu, "Additive Manufacturing of AlSi10Mg Alloy Using Direct Energy Deposition: Microstructure and Hardness Characterization," *J. Therm. Spray Technol.*, vol. 26, no. 4, pp. 587–597, 2017, doi: 10.1007/s11666-016-0495-4.

[6] X. Wang, L. Li, J. Qu, and W. Tao, "Microstructure and mechanical properties of laser metal deposited AlSi10Mg alloys," *Mater. Sci. Technol. (United Kingdom)*, vol. 35, no. 18, pp. 2284–2293, 2019, doi: 10.1080/02670836.2019.1674022.

[7] F. Lv, L. Shen, H. Liang, D. Xie, C. Wang, and Z. Tian, "Mechanical properties of AlSi10Mg alloy fabricated by laser melting deposition and improvements via heat treatment," *Optik (Stuttg).*, vol. 179, pp. 8–18, 2019, doi: 10.1016/j.ijleo.2018.10.112.

[8] G. Truppel, M. Rosa, M. Pereira, and P. Wendhausen, "Laser power influence on track's geometry and microstructure aspects of Fe and Sn-based alloy processed by directed energy deposition," *J. Laser Appl.*, vol. 32, p. 32002, 2020, doi: 10.2351/7.0000092.

[9] F. R. Kaschel, M. Celikin, and D. P. Dowling, "Effects of laser power on geometry, microstructure and mechanical properties of printed Ti-6Al-4V parts," *J. Mater. Process. Technol.*, vol. 278, p. 116539, Apr. 2020, doi: 10.1016/J.JMATPROTEC.2019.116539.

[10] H. El Cheikh, B. Courant, J. Y. Hascoët, and R. Guillén, "Prediction and analytical description of the single laser track geometry in direct laser fabrication from process parameters and energy balance reasoning," *J. Mater. Process. Technol.*, vol. 212, no. 9, pp. 1832–1839, Sep. 2012, doi: 10.1016/J.JMATPROTEC.2012.03.016.

[11] J. CHEN, W. HOU, X. WANG, S. CHU, and Z. YANG, "Microstructure, porosity and mechanical properties of selective laser melted AlSi10Mg," *Chinese J. Aeronaut.*, vol. 33, no. 7, pp. 2043–2054, Jul. 2020, doi: 10.1016/J.CJA.2019.08.017.

[12] H. Tan, D. Hao, K. Al-Hamdani, F. Zhang, Z. Xu, and A. T. Clare, "Direct metal deposition of TiB2/AlSi10Mg composites using satellited powders," *Mater. Lett.*, vol. 214, pp. 123–126, Mar. 2018, doi: 10.1016/J.MATLET.2017.11.121.

[13] Y. Gao, J. Zhao, Y. Zhao, Z. Wang, H. Song, and M. Gao, "Effect of processing parameters on solidification defects behavior of laser deposited AlSi10Mg alloy," *Vacuum*, vol. 167, no. May, pp. 471–478, 2019, doi: 10.1016/j.vacuum.2019.06.042.